BIOCHEMISTRY
including biophysical chemistry & molecular biology

Article

pubs.acs.org/biochemistry

Structural Basis for NHERF1 PDZ Domain Binding

Tatyana Mamonova,[†,‡] Maria Kurnikova,[‡] and Peter A. Friedman*[,†]

[†]Laboratory for G Protein-Coupled Receptor Biology, Department of Pharmacology & Chemical Biology, University of Pittsburgh School of Medicine, Pittsburgh, Pennsylvania 15261, United States

[‡]Department of Chemistry, Carnegie Mellon University, Pittsburgh, Pennsylvania 15213, United States

Supporting Information

ABSTRACT: The Na^+/H^+ exchange regulatory factor-1 (NHERF1) is a scaffolding protein that possesses two tandem PDZ domains and a carboxy-terminal ezrin-binding domain (EBD). The parathyroid hormone receptor (PTHR), type II sodium-dependent phosphate cotransporter (Npt2a), and β2-adrenergic receptor (β2-AR), through their respective carboxy-terminal PDZ-recognition motifs, individually interact with NHERF1 forming a complex with one of the PDZ domains. In the basal state, NHERF1 adopts a self-inhibited conformation, in which its carboxy-terminal PDZ ligand interacts with PDZ2. We applied molecular dynamics (MD) simulations to uncover the structural and biochemical basis for the binding selectivity of NHERF1 PDZ domains. PDZ1 uniquely forms several contacts not present in PDZ2 that further stabilize PDZ1 interactions with target ligands. The binding free energy (ΔG) of PDZ1 and PDZ2 with the carboxy-terminal, five-amino acid residues that form the PDZ-recognition motif of PTHR, Npt2a, and β2-AR was calculated and compared with the calculated ΔG for the self-association of NHERF1. The results suggest that the interaction of the PTHR, β2-adrenergic, and Npt2a involves competition between NHERF1 PDZ domains and the target proteins. The binding of PDZ2 with PTHR may also compete with the self-inhibited conformation of NHERF1, thereby contributing to the stabilization of an active NHERF1 conformation.

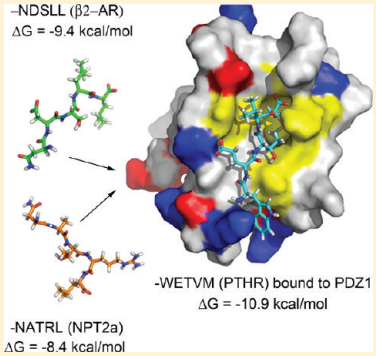

The Na^+/H^+ exchange regulatory factor-1 (NHERF1), known also as the 50-kDa ezrin-binding protein (EBP50), is a cytoplasmic scaffolding protein that assembles and regulates G protein-coupled receptors and other membrane-delimited proteins with signaling enzymes and cellular structural elements promoting the organization of functional macromolecular complexes.[1−3] NHERF1 consists of two tandem postsynaptic density 95/disk large/zona occludens (PDZ) domains and an ezrin-binding domain (EBD). The PDZ domains are globular structures comprising about 90 residues that mediate protein−protein interactions by binding heterologously to target proteins through short amino acid motifs at their carboxy-terminus (CT).[4,5] Class 1 motifs take the form D/E-S/T-X-Φ, where X is promiscuous and Φ is typically a hydrophobic residue such as L, I, V, or M.[6] By convention, the motif is numbered from position zero, which is the carboxy-terminal residue. The PDZ domains additionally engage in *cis* interactions to form homo- or heterodimers and bind to other proteins possessing PDZ domains.[7−9] The mechanism by which ligands associate with PDZ1 or PDZ2 is believed to be comparable.[10] The primary driving force for ligand−PDZ interactions is an ensemble of contacts between the carboxy-terminal carboxylate group of the ligand with amino acid residues forming the carboxylate-binding loop and the β2 strand of the PDZ domain.[11] Despite their apparent similarity, NHERF1 PDZ domains largely interact with dissimilar PDZ-binding partners and exhibit distinct affinities for them.[12−18] Most ligands, such as the cystic fibrosis transmembrane conductance regulator (CFTR), purinergic P2Y1 receptor, G-protein-coupled receptor kinase 6 (GRK6A), platelet-derived growth factor receptor (PDGFR), B1 subunit of the H^+ATPase, type II sodium-dependent phosphate cotransporters (Npt2a), and the β2-adrenergic receptor (β2-AR) bind to PDZ1.[19] The interaction with Npt2a regulates renal phosphate transport.[20] Binding involves three residues of the carboxy-terminal tail (TRL binding motif) of Npt2a.[21] PDZ1 binds with high affinity to the β2-AR and the CFTR four-residue carboxy-terminal motif (DSLL and DTRL, respectively), and moderately to the P2Y1 receptor tail (DTSL).[17,22] The association with the H^+ATPase occurs by means of the four-residue carboxy-terminal motif (DTAL).[23] In contrast to PDZ1, the PDZ2 domain reportedly interacts only with a few proteins.[16,24] Aquaporin 9 (AQP9) containing an SVIM motif binds to both PDZ domains of NHERF1 though with higher affinity for PDZ1.[25] An especially important function of NHERF1 is to regulate ligand bias, trafficking, and signaling of the parathyroid hormone receptor (PTHR).[26−33] The PTHR, through its carboxy-terminal PDZ-recognition motif (ETVM), binds to both PDZ1 and PDZ2 of NHERF1.[34,35] Furthermore, the NHERF1 PDZ2 domain interacts with its cognate carboxy-terminus, which is itself a PDZ ligand (FSNL).[36] Preliminary

Received: August 4, 2011
Revised: March 16, 2012
Published: March 19, 2012

immunoblot data (unpublished results) indicate that Npt2a interacts with PDZ2, albeit to a markedly lower extent compared to PDZ1. Similar observations have been reported recently.[37]

The structural basis for the binding preferences of PDZ1 and PDZ2 is not understood. The primary goal of this study was to uncover the structural basis for these binding preferences by theoretically analyzing the determinants of the specific binding of PDZ1 and PDZ2 and to compare their binding affinities for identical and divergent partners. We focused on systems that are biologically productive and for which there is experimental evidence of such interactions. Using molecular dynamics (MD) simulations, we demonstrate that in addition to the well-defined key interactions between PDZ1 or PDZ2 domains and carboxy-terminal PDZ-binding motifs,[10,11] PDZ1 forms several unique contacts not found in PDZ2 that further stabilize interactions between PDZ1 and target ligands. To support our observations and give a new insight into the problem regarding the affinity of interactions between PDZ1 or PDZ2 and target ligands, we estimated the binding free energy (ΔG) of PDZ1 to the carboxy-terminal, five-amino acid fragments of PTHR, Npt2a, and β2-AR and PDZ2 to the carboxy-terminal, five-amino acid fragments of PTHR. Our calculations demonstrate that PDZ1 has a higher binding affinity to the studied peptides than that of PDZ2. PDZ2 binds −LFSNL (the dash indicates the presence of upstream sequence), the NHERF1 EB domain, with comparable binding energy as does PDZ2 to −WETVM, the PTHR PDZ ligand. This important finding implies that the self-associated conformation of NHERF1 could control NHERF1−receptor interactions, screen a number of proteins containing a PDZ-recognition motif, interact with receptors with higher binding affinity, and, in so doing, regulate downstream cellular signaling pathways.

METHODS

System Modeling. The starting molecular structure was modeled on the basis of the NHERF1 PDZ1−β2-AR complex (PDB code: 1GQ4, 1.9 Å resolution). The PDZ1−β2-AR crystal structure includes head-to-tail polymers of PDZ1 molecules with the carboxy-terminal pentapeptide extension of one chimeric PDZ1 molecule serving as a ligand for a neighboring PDZ1.[11] In order to obtain a complex, we extracted a dimer and cut off the NDSLL tail. Thus, the PDZ1 domain (residues 10−94) fused to the β2-AR carboxyl-terminal sequence N^{95}DSLL^{99}. Water molecules are not involved in the PDZ−ligand interactions and were removed from the crystal structure. All missing hydrogen atoms were added using HARLEM (Hamiltonian for response properties of large molecules).[38] The carboxyl-terminal residue Leu refers to position 0 of the −NDSLL ligand. The neutral form of the peptide amino termini was used to avoid introducing artificial positive charges that could bias the MD calculation. All initial files for the MD simulation of ligand bound PDZ1 domain were generated by Leap (module of AMBER 9[39]). The overall charge of the system was kept neutral. Sodium ions were added to neutralize the systems when necessary. The TIP3P water model was used for the water molecules.[40] Computational details are summarizing in Table S1 of the Supporting Information. The protocol for minimization, equilibration, and production MD simulations was as follows.

Before each equilibration simulation was run, the potential energy of each system was minimized by 100 steps steepest descent minimization followed by 400 steps of conjugate gradient minimization. Then a 100 ps MD simulation was performed with protein atoms controlled in space by a harmonic restraint with a force constant of 100 kcal mol^{-1} Å^{-2} to allow the water box size to shrink to its final dimensions, preventing a low water density. The temperature of each system was gradually increased to T = 300 K at a constant pressure of 1 atm. Then, each system was equilibrated over 100 ps in the *NPT* ensemble with weak restraints of 10, 5, 2, 1, and 0.1 kcal mol^{-1} Å^{-2}. Next, only the C_α atoms of the amino-terminal residue of the ligand were kept restrained with a weak force constant of 0.1 kcal mol^{-1} Å^{-2}, while all other atoms were free to move. After that, the equilibration was performed in the *NVT* ensemble with a weak force constant of 0.1 kcal mol^{-1} Å^{-2}. All production runs were done in the *NVT* ensemble. During the production runs, the entire complex was unconstrained except for the three backbone (0.1 kcal mol^{-1} Å^{-2} for N, C, C_α) atoms at the amino-terminal residue of the ligand to prevent its diffusion away from the complex. The equilibrium structure of PDZ1−NDSLL was used to build PDZ1 in the bound state with the −NDSLL/Val (Figure S1A of the Supporting Information), the −NDSLL/Ala (Figure S1B of the Supporting Information), the −WETVM (CT of PTHR) (Figure 1A), or the −NATRL (CT of Npt2a) peptide (Figure 2 and Figure S1C of the Supporting Information). All peptides in this study were truncated to their corresponding carboxy-terminal 5 residue motifs, as the residues upstream from position −4 are solvent-exposed, and their contribution in the protein−peptide interaction was assumed to be negligible. For −NDSLL/Val or −NDSLL/Ala, only Leu^0 was replaced by Val or Ala, respectively. The −NDSLL ligand was replaced by −WETVM or −NATRL. All replacements were made in Leap (module of AMBER 9[39]). In all cases, the ligand was aligned in an antiparallel orientation with the PDZ1 β2 strand. The carboxy-terminal residues Met or Leu refer to position 0 of PTHR and Npt2a, respectively.

To build PDZ2 complexed with the carboxy-terminal fragment of NHERF1 (−LFSNL) [EB ligand] or PTHR (−WETVM), we used the equilibrium structure of the PDZ1−NDSLL complex as a template. PDZ1 and PDZ2 have high pairwise sequence similarities (Figure S2 of the Supporting Information), share similar structures, and conserved ligand-binding pockets. The equilibrium structure of the PDZ2 domain was derived after equilibration of the crystal structure (PDB code: 2OZF, residues Ser148−Leu239, 1.5 Å resolution) in the MD simulation as described above. All C_α atoms of the target PDZ2 domain were superimposed with the C_α atoms of the PDZ1 protein in the PDZ1−NDSLL complex. This resulted in a very close superposition of PDZ1 and PDZ2 with an rmsd value of 1.6 Å (the 4 flexible amino- and 3 carboxy-terminal amino acid residues are not included in this value). Then, all atoms of PDZ1 were replaced by PDZ2. Finally, the −NDSLL peptide was replaced with −LFSNL for the EB ligand, or to −WETVM for the CT of PTHR, in Leap (module of AMBER 9[39]). In both cases, the ligand was aligned in an antiparallel orientation with the PDZ2 β2 strand. The carboxyl-terminal residues Met or Leu refer to position 0 of the PTHR and EB ligand motifs (Figure 3). Both PDZ2−LFSNL and PDZ2−WETVM were solvated with water (TIP3P) (Leap module of AMBER 9[39]). The protocol for minimization, equilibration, and production MD simulation of each system was performed as described above. All computational details are summarized in Table S1 of the Supporting Information. Both PDZ2-ligand structures are presented in Figure S1D,E of the Supporting Information.

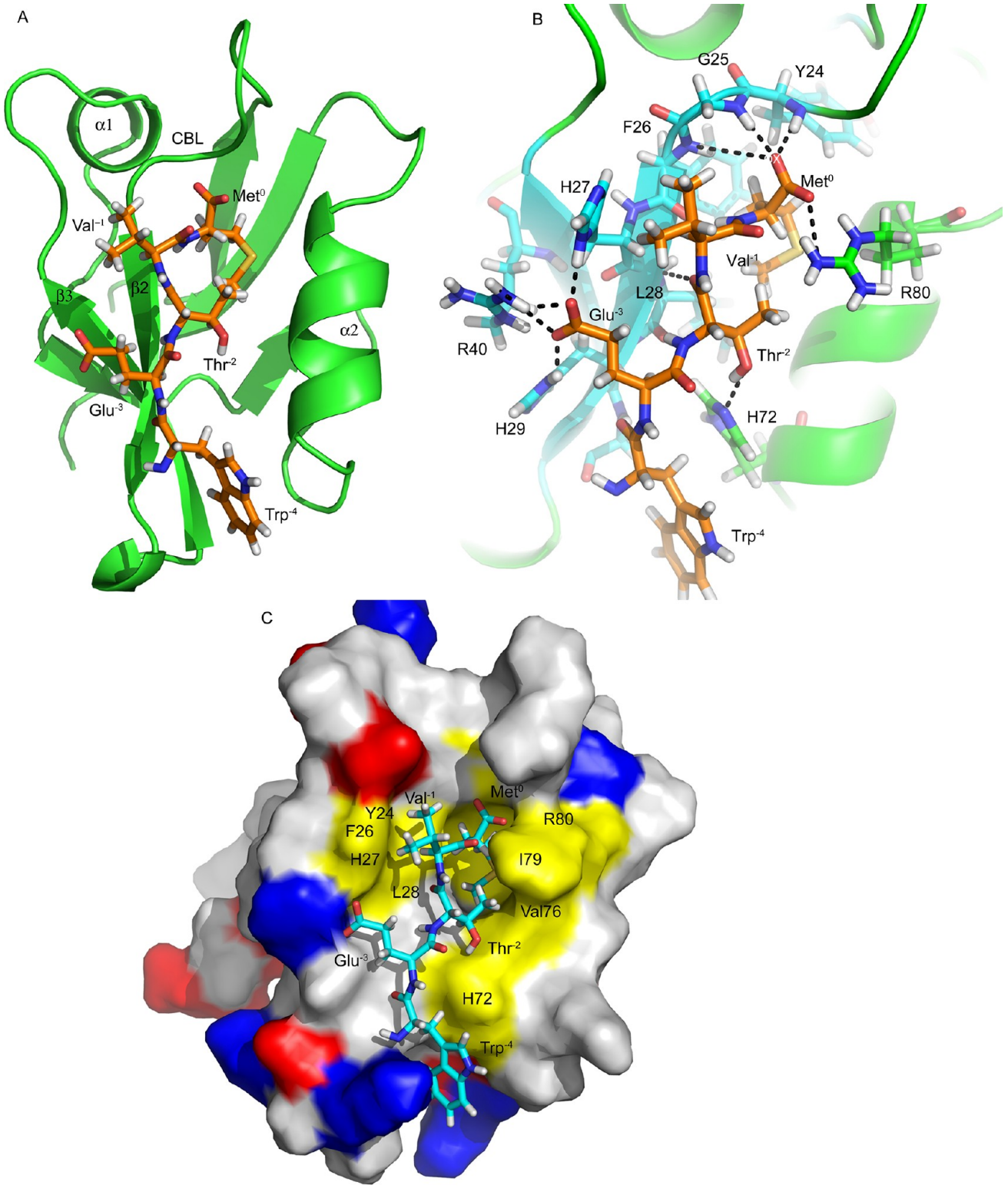

Figure 1. Structure of the NHERF1 PDZ1 domain with the −WETVM (PTHR) ligand. (A) Ribbon diagram shows the structure of the PDZ1−ligand complex with labeled β-strands β2 and β3, helixes α1 and α2, and the CBL−carboxylate-binding loop. Hydrogen atoms are white, oxygens are red, and nitrogens are blue. The −WETVM ligand is colored in orange. (B) Zoomed view of the binding pocket. Hydrogen bonds between the −WETVM ligand and PDZ1 are shown as black dashes. (C) Surface representation of the hydrophobic pocket. Residues forming hydrophobic interactions with the ligand (cyan) are colored in yellow; basic, acidic, and neutral residues are shown in blue, red, and gray, respectively.

Two additional mutated complexes were generated. In the first, Glu43 was replaced with Asp in the PDZ1−NATRL complex (Figure 4A). In the second mutant, Ala replaced His27 in the PDZ1−WETVM complex (Figure 5A). Both mutated systems were prepared by the Leap module of AMBER 9.[39] Each system was minimized before the PDZ1E43D−NATRL

dx.doi.org/10.1021/bi201213w | *Biochemistry* 2012, 51, 3110−3120

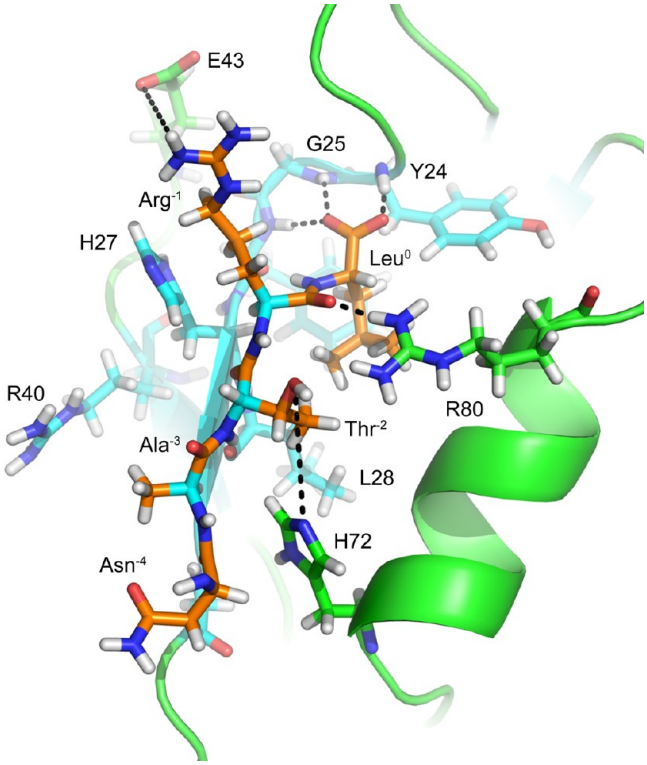

Figure 2. Zoomed view of the binding pocket of the PDZ1−NATRL complex. The −NATRL (NPT2a) ligand (colored in orange). For an explanation of the color code, see the legend to Figure 1.

or PDZ1H27A−WETVM complex was run. The protocol for minimization, equilibration, and production MD simulations was used as described above. All computational details are summarized in Table S1 of the Supporting Information.

Simulation Parameters. The equilibration and production MD simulations were performed using the AMBER 10[41] molecular modeling package (PMEMD module) with the Cornell et al. force-field.[42] The equilibrium temperature was 300 K in all simulations. This was controlled using the Berendsen thermostat.[43] Periodic boundary conditions were applied. An isothermal isobaric ensemble (NPT) was used to adjust the solvent density. Then equilibration and production simulations were performed in the *NVT* ensemble. The particle mesh Ewald (PME) method[44] was used to compute long-range electrostatic and Lennard−Jones interactions with 12 Å. An integration time step was 2 fs for all MD simulations. The SHAKE algorithm was applied.[45] The trajectory data were written at 2 ps intervals during both equilibration and production runs.

Analysis of MD Trajectories. The equilibration of the MD trajectories was monitored by computing the root-mean-square deviation (rmsd) of the C_α atoms of the entire complex and the C_α atoms of the ligand, and the C_α atoms of residues formed a binding pocket (Tyr24, Gly25, Phe26, Leu28, Val76 and Ile79 of PDZ1; Tyr164, Gly165, Phe166, Leu168, Val216, and Ile219 of PDZ2) from their initial positions (Table S1 of the Supporting Information). The equilibration process was sufficiently long (30−50 ns) to allow the relaxation of solvent molecules, loop residues, and ligands. For PDZ1-NDSLL/Ala, where only a side chain of Leu^0 was replaced by Ala^0 (Figure S1B of the Supporting Information), a 6.5 ns MD simulation was sufficient to equilibrate the mutated structure. Evolution of the rmsd values for the complexes studied is presented in Figures S3−S6 of the Supporting Information. To assess relative mobility of the protein regions in the course of the MD simulations, the root mean square fluctuation (RMSF) of each C_α atom as a function of residue number was calculated with respect to its average position in the structure (Figure S7 of the Supporting Information).

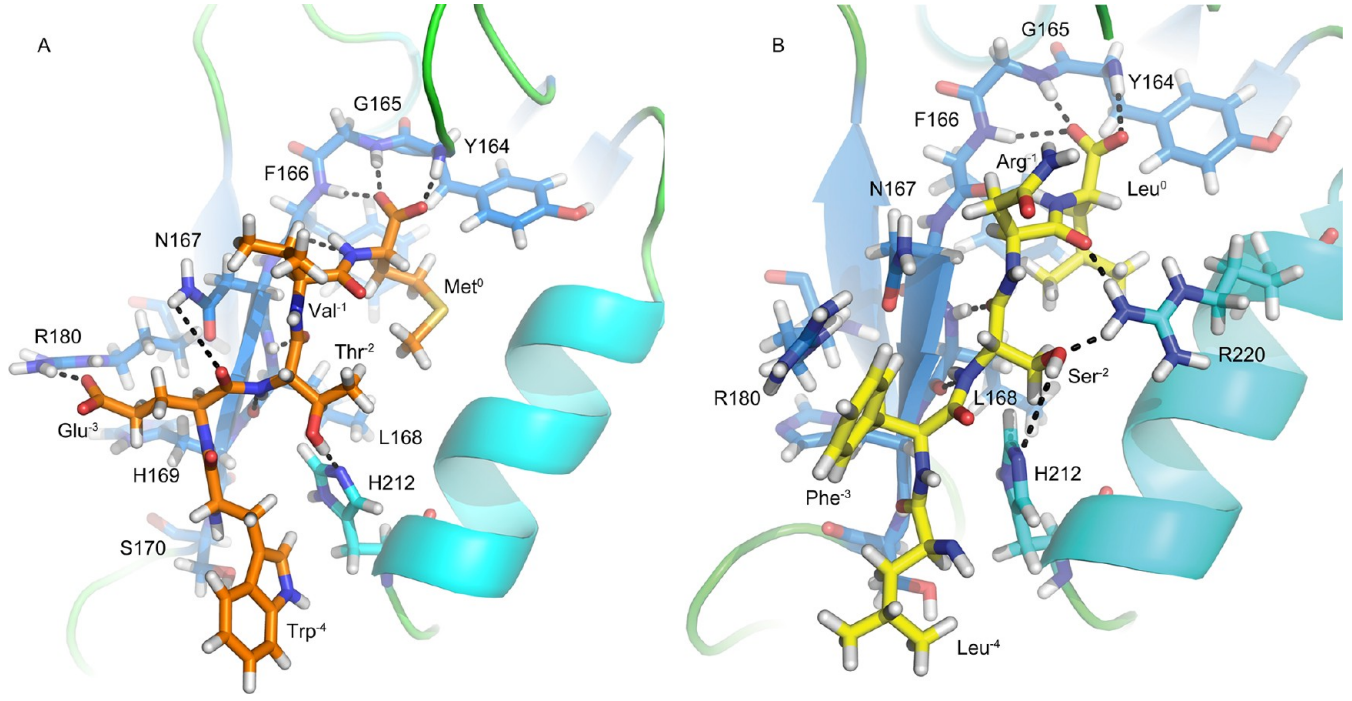

Figure 3. Enlarged representation of the binding pocket of PDZ2. (A) H-bonds with the −WETVM ligand (colored in orange); (B) H-bonds with the −LFSNL ligand (colored in yellow). For an explanation of the color code, see the legend to Figure 1.

dx.doi.org/10.1021/bi201213w | *Biochemistry* 2012, 51, 3110−3120

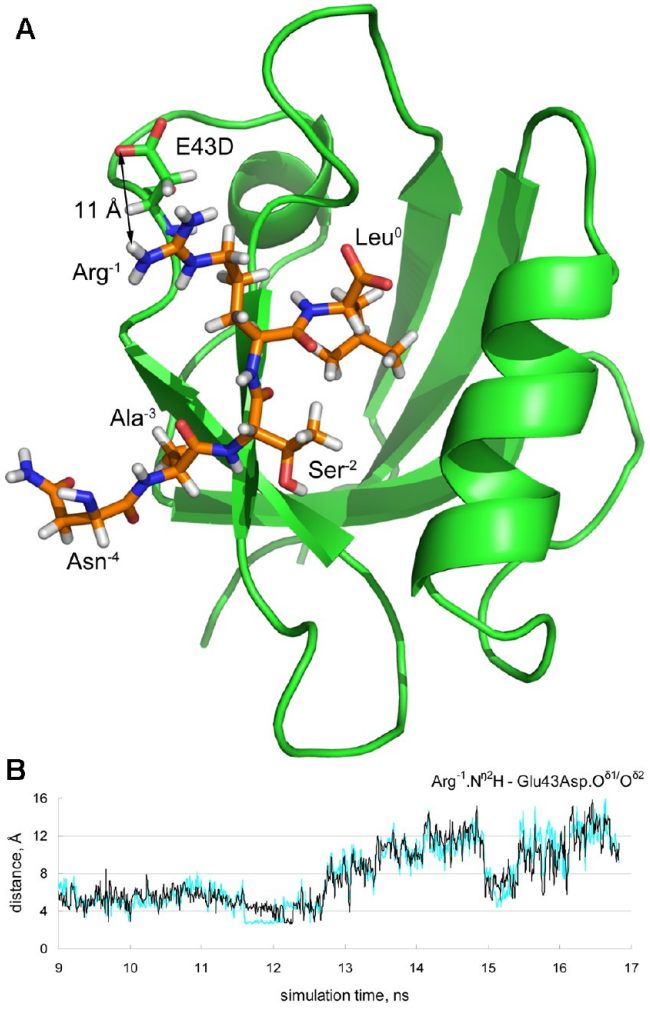

Figure 4. Glu43Asp mutation disrupts the interaction between Arg^{-1} of the −NATRL ligand and Glu43Asp of PDZ1. (A) Ribbon diagram shows the structure of the PDZ1E43D−NATRL complex. (B) The evolution of the distance between $Arg^{-1}.N^{\eta 2}H$ and Glu43Asp. $O^{\delta 1}$ (black)/$O^{\delta 2}$ (cyan) along the MD trajectory.

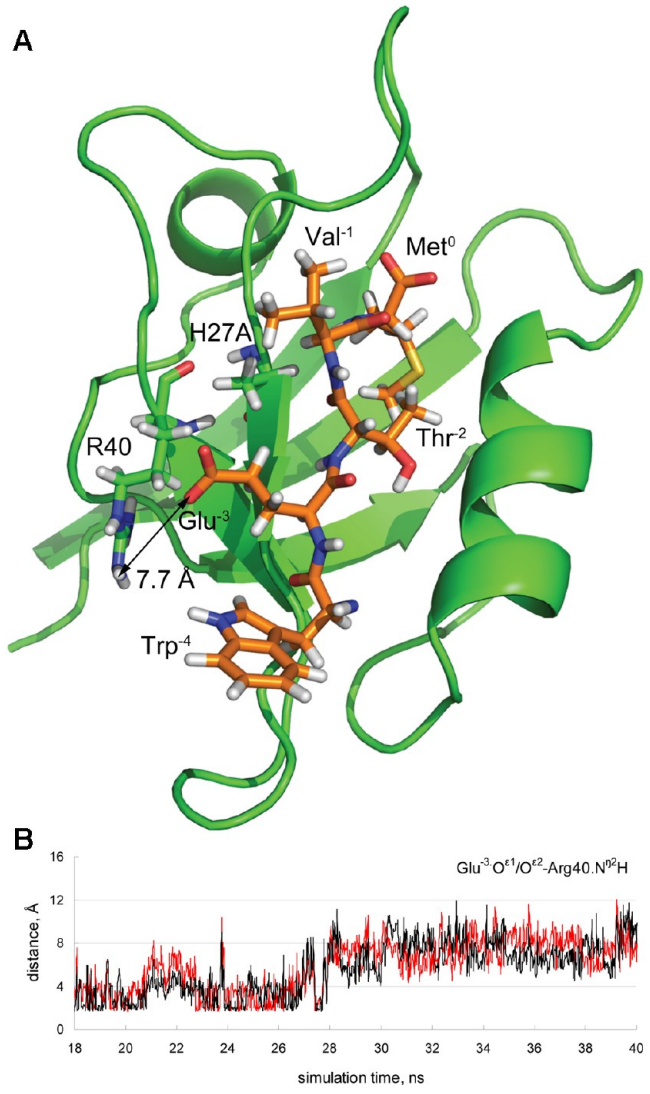

Figure 5. His27Ala mutation in the PDZ1−WETVM complex disrupts the interaction between Glu^{-3} of the −WETVM ligand and Arg40 of PDZ1. (A) Ribbon diagram shows the structure of PDZ1H27A−WETVM complex. (B) The evolution of the distance between $Glu^{-3}.O^{\varepsilon 1}$ (black)/$O^{\varepsilon 2}$ (red) and $Arg40.N^{\eta 2}H$ along the MD trajectory.

Binding Free Energy Calculation (ΔG). The PDZ−ligand binding free energy is approximated using the solvated interaction energy (SIE) formalism implemented in the Sietraj program[46]

$$\Delta G_{bind}^{calc} = \underbrace{E_{inter}^{C} + \Delta G_{bind}^{R}}_{\Delta G_{bind}^{elec}} + \underbrace{E_{inter}^{vdw} + \Delta G_{bind}^{npsol}}_{\Delta G_{bind}^{np}} \quad (1)$$

where E_{inter}^{C} and E_{inter}^{vdw} are the intramolecular Coulomb and van der Waals interactions energies in the bound state, respectively. The electrostatic contribution of the solvation free energy to binding, ΔG_{bind}^{R}, is the change in the reaction field energy between the bound and free states. The nonpolar contribution of the solvation free energy to binding, ΔG_{bind}^{npsol}, is the change in the nonelectrostatic solvation free energy (the solute−water van der Waals energy plus the cavitation cost in water) between the bound and free states. The above decomposition technique is similar to MD/PBSA[47] and has been applied successfully by us for the ligand binding domain of GluR2.[48] Recent publications show that the SIE method used in computational studies of complexes of protein and small molecule ligands yields binding affinity predictions that agree well with the corresponding experimental data,[49,50] whereas the binding free energies calculated by using the MM/GBSA method are much lower than the corresponding experimental binding free energies.[50] In our study, the SIEs were collected at 20 ps intervals over a 5 ns MD trajectory and average energies calculated. All sodium ions and water molecules were removed for the SIE calculation. Variation of binding energies with simulation time for the PDZ1−ligand complexes is presented in Figure S8 of the Supporting Information.

Hydrogen Bond Analysis. Calculation of noncovalent bonds was carried out using HARLEM and Python scripts as described elsewhere.[51] In short, to generate a list of potential hydrogen bonds (H-bond), salt bridges, or hydrophobic contacts, all possible acceptors within 6 Å from a donor atom were monitored over a 5 ns MD trajectory. When the geometric criteria were satisfied for a pair of atoms, an H-bond was registered. The existence of an H-bond was defined by the

dx.doi.org/10.1021/bi201213w | Biochemistry 2012, 51, 3110−3120

following geometric criteria:[52−54] the donor−acceptor distance is within 3.6 Å, the hydrogen−acceptor distance is within 2.6 Å, and the donor−hydrogen−acceptor angle is >90°. Salt bridges were registered when the Asp or Glu side chain oxygen atoms were within 4.6 Å from the nitrogen atom of the Arg, Lys, and His side chain; the hydrogen−acceptor distance is within 3.6 Å, and the donor−hydrogen−acceptor angle is >80°. A hydrophobic contact was defined when any two pairs of carbon atoms or any carbon and any sulfur atom were at a distance <4 Å. All interactions persisting more than 50% along a 5 ns MD trajectory are included in Tables 1−3.

Table 1. Hydrophobic Interactions between PDZ1 or PDZ2 and the Tested Ligands over a 5 ns MD Trajectory

ligand/position		PDZ1	PDZ2
(−NDSLL)	Leu^0	Tyr24, Phe26, Leu28, Val76, Ile79	
	Leu^{-1}	His27	
(−NATRL)	Leu^0	Tyr24, Phe26, Leu28, Val76, Ile79	
(−WETVM)	Met^0	Tyr24, Phe26, Leu28, Val76, Arg80[a], Ile79	Phe166, Val216, Ile219, Arg220
	Val^{-1}	His27	
	Trp^{-4}	His72	His212
(−LFSNL)	Leu^0		Tyr164, Phe166, Leu168, Val216, Ile219, Arg220
	Phe^{-3}		His169, Arg180
	Leu^{-4}		His212

[a]The aliphatic side chain of Arg80 of PDZ1 and Arg220 of PDZ2 forms hydrophobic contacts with the side chains Met^0 or Leu^0.

Table 2. Hydrogen Bond Interactions between PDZ1 or PDZ2 and the Tested Ligands over a 5 ns MD Trajectory

ligand/position		PDZ1	PDZ2
(−NDSLL)	Leu^0	Tyr24, Gly25, Phe26, Arg80	
	Leu^{-1}	Arg80	
	Ser^{-2}	Leu28, His72	
	Asn^{-4}	Gly30	
(−NATRL)	Leu^0	Tyr24, Gly25, Phe26	
	Arg^{-1}	Arg80	
	Thr^{-2}	Leu28, His72	
(−WETVM)	Met^0	Tyr24, Gly25, Phe26, Arg80	Tyr164, Gly165, Phe166
	Val^{-1}		Leu168, His212
	Thr^{-2}	Leu28, His72	Asn167
	Glu^{-3}		
(−LFSNL)	Leu^0		Tyr164, Gly165, Phe166, Arg220
	Asn^{-1}		Asn167, Arg220
	Ser^{-2}		Leu168, His212

Table 3. Salt Bridge Interactions of PDZ1 and PDZ2 at $Site^{-1}$ and $Site^{-3}$ of the Tested Ligands over a 5 ns MD Trajectory

ligand/position		PDZ1	PDZ2
(−NDSLL)	Asp^{-3}	Arg40	
		His27	
(−WETVM)	Glu^{-3}	Arg40	Arg180
		His27	
		His29	
(−NATRL)	Arg^{-1}	Glu43	

RESULTS

Overall Characteristics. MD simulations were performed for both PDZ1 and PDZ2 domains of NHERF1. The equilibration of the MD trajectories was monitored as the time dependence of the rmsd of the C_α atoms from their initial positions for the whole complex, binding pocket, and ligand. Figures S3−S6 of the Supporting Information present evolution of the rmsd of the C_α atoms with respect to the initial conformation during equilibration simulation for the PDZ1−WETVM, PDZ1−NATRL, PDZ2−WETVM, and PDZ2−LFSNL complexes. The average rmsd values of the C_α atoms of the complex, binding pocket, and ligands throughout the equilibration and production MD simulations are summarized in Table S1 of the Supporting Information. The equilibration time varied among systems, ranging from 30 to 50 ns (Table S1 of the Supporting Information). The superposition of the equilibrated the PDZ1−ligand complexes reveals small differences among PDZ1−NDSLL, PDZ1−WETVM, and PDZ1−NATRL systems. The liganded PDZ1 structures are very stable with the overall rmsd values of the C_α atoms ranging from 1.3 to 2.2 Å from the minimized structure throughout the production MD simulation. The rmsd values of the C_α atoms for the liganded PDZ2 structures are 1.1 Å. In the case of PDZ2, it should be noted that, in contrast to the PDZ1−ligand systems discussed above, the starting structure was derived from X-crystallography (PDB code: 2OZF) and equilibrated in MD simulation. This PDZ2 equilibrium structure was then used for the simulations of the PDZ2−ligand systems. This difference may explain the observed higher rmsd values of the C_α atoms for the PDZ1−ligand systems compared to those of PDZ2. The binding of the ligands does not cause conformational changes of the binding pocket of either PDZ1 or PDZ2. The rmsd values stay within the range of 0.4−0.7 Å from the minimized structures throughout the equilibration phase and indicate the ability of PDZ1 and PDZ2 to accommodate ligands with different side chains and polarity. The rmsd values of the C_α atoms of the peptide ligands (NDSLL, WETVM, and LFSNL) range from 0.5 to 0.9 Å from the minimized structures throughout the equilibration phase and production simulation. This stability is due to a strong network of interactions that tightly binds the ligands. For all investigated systems, the largest conformational changes were observed in the carboxylate-binding loop (Gly20-Asn22 of PDZ1 and Gly160-Ser162 of PDZ2), $\beta2$-$\beta3$ (Lys32−Lys34 of PDZ1 and Lys172−Lys174 of PDZ2) loops. The local mobility of each protein residue obtained from the RMSF calculation of the C_α atoms with respect to the average structure is presented in Figure S7 of the Supporting Information. Formation of PDZ2−WETVM or PDZ2−LFSNL complexes stabilizes the $\beta2$−$\beta3$ loop only partially (Figure S7B of the Supporting Information).

Evolution of rmsd of the C_α atoms with respect to the initial conformation during equilibration simulation for the mutated PDZ1−NDSLL/Ala and PDZ1−NDSLL/Val systems is presented in Figures S9−S10 of the Supporting Information. The average rmsd values of the C_α atoms from the initial structures along the equilibration phase and production simulation are shown in Table S1 of the Supporting Information.

Comparison of Target Ligand $Site^0$ and $Site^{-2}$ of PDZ1 and PDZ2. To understand better the selectivity of PDZ1 and PDZ2 domains for their target ligands, we compared the PDZ1−NDSLL, PDZ1−WETVM, PDZ1−NATRL, PDZ2−WETVM, and PDZ2−LFSNL structures derived from the equilibrium MD simulations. Both PDZ1 and PDZ2 form extensive contacts with the bound ligands including specific

dx.doi.org/10.1021/bi201213w | Biochemistry 2012, 51, 3110−3120

interactions for class I PDZ domains.[55] Figures 1B, 2, and 3 reveal residues of PDZ1 and PDZ2 involved in these contacts. All noncovalent interactions observed more than 50% along a 5 ns MD trajectory are summarized in Tables 1−3. The carboxy-terminal carboxylate group of Met^0 and Leu^0 forms hydrogen bonds with the backbone amides of the carboxylate-binding loop (Tyr24, Gly25, and Phe26 of PDZ1 (Figures 1B and 2); Tyr164, Gly165, and Phe166 of PDZ2 (Figure 3 A,B)). Representation of the PDZ1 binding pocket occupied by the −WETVM ligand is shown in Figure 1B,C. This type of interaction is conserved among the PDZ family.[11] The aliphatic side chain of Met^0 or Leu^0 is buried deep within a hydrophobic pocket of PDZ1 and forms multiple hydrophobic contacts with the side chains of Tyr24, Phe26, Leu28, Val76, Ile79, and Arg80 (Figures 1B and 2). We observed similar contacts between Leu^0/Met^0 and Tyr164, Phe166, Leu168, Val216, Ile219, and Arg220 of PDZ2 (Figure 3A,B). However, the hydrophobic pocket poorly accommodates ligands with a small side chain at position 0. Ala^0 of −NDSLL/A, for example, forms few interactions with Phe26 in PDZ1.

In all structures investigated, the hydroxyl oxygen of Thr^{-2} or Ser^{-2} forms a hydrogen bond with a hydrogen attached to $N^{\varepsilon 2}$ of His72 in the $\alpha 2$ helix of PDZ1 (Figures 1B and 2) or His212 in the $\alpha 2$ helix of PDZ2 (Figure 3). In addition, there is a bifurcate hydrogen bond between Ser^{-2} or Thr^{-2} and the backbone oxygen and amide proton of Leu28 of the $\beta 2$ strand of PDZ1 (Figures 1B and 2) and Leu168 of the $\beta 2$ strand in PDZ2 (Figure 3). The aliphatic portion of the Thr^{-2} or Ser^{-2} side chain is in hydrophobic contact with Val76 of PDZ1 and Val216 of PDZ2.

Comparison of Site^{-1} and Site^{-3} of Target Ligands for PDZ1 and PDZ2. In the PDZ1−NATRL complex, the guanidino group of Arg^{-1} forms electrostatic interactions with $O^{\varepsilon 1}$/$O^{\varepsilon 2}$ of Glu43 (Figure 2). Unexpectedly, the C^{γ} atom of Arg^{-1} may form a hydrophobic contact with the $C^{\delta 2}$ atom of His27 of $\beta 2$. In contrast, PDZ2 contains Asp183 in the $\beta 3$ strand and Asn167 in the $\beta 2$ strand, which do not interact with Val^{-1} of PDZ2−WETVM. Our findings show that the carboxylic group of Glu^{-3}.$O^{\varepsilon 1}$/$O^{\varepsilon 2}$ of PDZ1−WETVM, PDZ2−WETVM, or Asp^{-3}.$O^{\delta 1}$/$O^{\delta 2}$ of PDZ1−NDSLL establishes electrostatic interactions with hydrogens attached to $N^{\eta 2}$ of Arg40 of PDZ1 (Figure 1B) or Arg180 of PDZ2 (Figure 3A). An example of the evolution of the distance between the carboxylic group of Glu^{-3} or Asp^{-3} and the hydrogen attached to $N^{\eta 2}$ Arg40 of PDZ1 over equilibration and production simulations is presented in Figures S11 and S12 (Supporting Information, right panel). The Glu^{-3}.$O^{\varepsilon 1}$/$O^{\varepsilon 2}$−Arg40.$N^{\eta 2}$H or Asp^{-3}.$O^{\delta 1}$/$O^{\delta 2}$−Arg40.$N^{\eta 2}$H distance fluctuates during equilibration and plateaus at 2 Å throughout the production simulation, indicating a stable salt bridge.

We further observed that the carboxylic group of Glu^{-3} or Asp^{-3} is involved in the interactions with the hydrogens attached to $N^{\delta 1}$ of His27 of PDZ1 (Figure 1B). Glu^{-3}.$O^{\varepsilon 1}$/$O^{\varepsilon 2}$ forms a stable salt bridge with His27 (see left panel, Figure S11 of the Supporting Information). Asp^{-3}.$O^{\delta 1}$/$O^{\delta 2}$ also interacts with His27 (see left panel, Figure S12 of the Supporting Information). However, these interactions are less stable than those between Glu^{-3} and His27. Calculation of hydrogen bonds shows (Table 3) that His29 of PDZ1 is also involved in the interaction with Glu^{-3} of −WETVM but much less with Asp^{-3} of −NDSLL.

Contribution of Target Ligand Site^{-4} to Binding of PDZ1 and PDZ2. Hydrogen bond analysis reveals (Table 1) that Trp and Leu at position −4 (PDZ1−WETVM, PDZ2−WETVM, and PDZ2−LFSNL), respectively, form hydrophobic contacts with His72 of PDZ1 or His212 of PDZ2. Asn^{-4} of −NDSLL establishes a backbone hydrogen bond with Gly30 of PDZ1 (Table 2). However, Asn^{-4} of −NATRL is not involved in such an interaction (Figure 2 and Figure S1C of the Supporting Information).

Simulation of PDZ1 His27Ala−WETVM and PDZ1Glu43Asp−NATRL Mutants. Table S1 of the Supporting Information lists the average rmsd values of both mutants as well as of the binding pockets and ligands over equilibration and production simulations with respect to the minimized structure. As one can see, both complexes are stable with the rmsd values in the range 1.4−1.6 Å. For the −NATRL ligand, we observed the highest rmsd value, which may indicate a loss of the interaction between PDZ1Glu43Asp and Arg^{-1} of NATRL (Figure 4A). To further validate these results, we calculated the distance between the Glu43Asp.$O^{\delta 1}$/$O^{\delta 2}$ atoms and the amino group of Arg^{-1}. The distance is illustrated in Figure 4B. As can be seen, the distance fluctuates between 3 and 8 Å during first 13 ns (Figure 4B). Then, the distance becomes more than 4.5 Å, indicating the loss of a salt bridge (Figure 4A,B).

In the case of PDZ1His27Ala, the replacement affects the interaction between Glu^{-3} of −WETVM and Arg40 of PDZ1 (Figure 5A). Figure 5B displays the evolution of the distance between Glu^{-3}.$O^{\varepsilon 1}$/$O^{\varepsilon 2}$ and $N^{\eta 2}$H of Arg40. The distance fluctuates between 2 and 8 Å over the first 28 ns of the MD simulation and then stabilizes at 7.3 Å, indicating the loss of a salt bridge between Glu^{-3} and Arg40 (Figure 5A,B).

Binding Energy between PDZ1, PDZ2, and Target Ligands. Free energy calculations have been performed to complement the hydrogen bond analysis. The SIE method (eq 1) was used. In all cases, computed free energies remain stable throughout the production MD simulation (Figure S8 of the Supporting Information). Table 4 summarizes the average binding free energies among PDZ1 and −WETVM, −NDSLL, and −NATRL, and among PDZ2 and −WETVM and −LFSNL. The free energy values were averaged over 250 snapshots taken at 20 ps intervals from the production MD simulations. The

Table 4. Binding Free Energy (kcal/mol) Depends on the Specific Ligand Sequence

ligand	PDZ1	PDZ2
−NDSLL	−9.4 ± 0.4[a]	none[c]
−NDSLV	−9.0	none
−NDSLA	−8.5	none
−NATRL	−8.4	possible[d]
E43D-NATRL	−8.2	
−WETVM	−10.9	−9.5
H27A-WETVM	−9.4	
−LFSNL		−8.8
−DTRL[b]	−8.2	none
−VQDTRL[b]	−8.8	−8.1

[a]The standard deviation was ±0.4 kcal/mol in all calculations. [b]Sequences correspond to the CFTR carboxy-terminus. Binding energies were calculated using an equation $\Delta G = -RT \ln K_d$, with the K_d values from ref 13. The PDZ2 construct includes both core and the flanking residues (248−299). [c]NHERF1 PDZ2 in the self-associated conformation prevents interaction with both CFTR and $\beta 2$-AR.[8,13] [d]A weak interaction was recently detected experimentally by us and others.[37]

results show that 200−250 snapshots are sufficient to estimate mean values with reasonable precision. In all cases, electrostatic contribution favors the PDZ1 or PDZ2 ligand association. The nonpolar interaction, particularly the van der Waals term, contributes favorably to the binding affinity of PDZ1 or PDZ2. The favorable nonpolar free energy terms are consistent with the structural feature of PDZ1 or PDZ2. As observed in PDZ−ligand binding, the peptide ligand is lodged in the hydrophobic binding pocket surrounded by the side chains of Tyr24, Gly25, Phe26, Leu28, Val76, or Ile79 of PDZ1 (Figures 1 and 2) and Tyr164, Gly165, Phe166, Leu168, Val216, and Ile219 of PDZ2 (Figure 3).

DISCUSSION

The present studies show that both PDZ1 and PDZ2 domains of NHERF1 recognize the carboxy-terminal five-residue motifs of selected proteins by virtue of interactions that span the entire surface of the binding groove. Most PDZ1 and PDZ2 interactions are established through the β2 strand and α2 helix.

Both PDZ1 and PDZ2 have a strict preference for hydrophobic residues such as Leu or Met at position 0. Replacement of Leu by Val or Ala at position 0 of the −NDSLL ligand lowers the binding energy (Table 4). Both side chains of Val^0 and Ala^0 are relatively short and do not fit tightly in the hydrophobic cavity. As a result, we observed weaker hydrophobic interactions between the side chain of Val^0 or Ala^0 and the side chain of Tyr 24, Phe26, Val76, and Ile79 of PDZ1.

His72 of PDZ1 and the orthologous His212 of PDZ2 form hydrogen bonds with Ser^{-2} or Thr^{-2} of the target ligands. This key interaction is specific for recognition by class I PDZ domains and is in good agreement with existing structural studies.[11,55] In addition, a bifurcate H-bond between Ser^{-2} or Thr^{-2} and Leu28 of PDZ1 and Leu168 of PDZ2 contributes to the binding.

Novel findings described here indicate that the formation of salt bridges between Arg40 in the β3 strand of PDZ1 and Glu^{-3} in PDZ1−WETVM or Asp^{-3} in PDZ1−NDSLL, as well as between Arg180 of the β3 strand of PDZ2 and Glu^{-3} in PDZ2−WETVM, importantly stabilize PDZ−ligand complexes. This interaction was also observed in the crystal structure of the NHERF1 complexes of PDZ1-β2-AR, NHERF1 PDZ1-PDGFR, and NHERF1 PDZ1-CFTR[11,55] and other members of the PDZ domain family.[56]

We hypothesized that His27 and His29 are essential for additional stabilization of PDZ1−ligand complexes, particularly when the ligand has a negatively charged residue at position −3. We found that the carboxylic group of Glu^{-3} of the −WETVM peptide is located between two imidazole rings of His27 and His29 of PDZ1 with which it forms hydrogen bonds (Figure S13 of the Supporting Information). To validate this result, we calculated the distance between $Glu^{-3}.O^{\epsilon1}/O^{\epsilon2}$ and $His27.N^{\delta1}H$. The distance fluctuates between 2 and 4 Å during equilibration and remains around 2 Å over production simulations, indicating a strong and stable salt bridge (left panel, Figure S11 of the Supporting Information). Formation of a salt bridge between Asp^{-3} and Arg40 and His27 of NHERF1 PDZ1 was detected in previous computational studies.[57,58] However, the authors did not provide details of these interactions. To demonstrate that His27 is essential for the formation a salt bridge between Glu^{-3} and Arg40, we replaced His27 with Ala. This substitution disrupted the interaction between Glu^{-3} and Arg40, as reflected by the dramatically increased distance between $Glu^{-3}.O^{\epsilon1}/O^{\epsilon2}$ and $N^{\eta2}H$ Arg40 (Figure 5B).

The electrostatic nature of the interaction between Glu^{-3} and Arg40, as well as that between Glu^{-3} and His27, significantly strengthens the total binding energy. Thus, PDZ1 binds the −WETVM peptide with the highest binding energy of −10.9 ± 0.4 kcal/mol. As expected, the binding energy between PDZ1H27A and −WETVM is lower (−9.0 ± 0.4 kcal/mol) compared to that of wild type PDZ1. For the −NDSLL ligand, His27 contributes more than His29 to stabilizing the PDZ1−NDSLL complex due to the formation of short contacts with Asp^{-3}. PDZ1 binds with the −NDSLL peptide with a binding free energy of −9.4 ± 0.4 kcal/mol.

It should be noted that Arg^{-1} of −NATRL (but not Val^{-1} or Leu^{-1} of −WETVM and −NDSLL, respectively) also forms electrostatic interactions. We observed multiple contacts between hydrogens at $N^{\eta2}$ and $N^{\eta2}$ of Arg^{-1} and a carboxylic group of Glu43 of PDZ1 (Table 3). To demonstrate that Glu43 in PDZ1 increases its binding capacity with position −1 of the −NATRL ligand, we replaced Glu43 with Asp. The results show that Glu43 and Asp43 differ significantly in their specificity to interact with Arg^{-1}. Calculation of hydrogen bonds reveals that Glu43Asp does not form interactions with Arg^{-1}. This may explain the high rmsd value for the −NATRL ligand in the PDZ1Glu43Asp−NATRL complex compared to the wild type structure. The estimated binding energy for the PDZ1Glu43Asp−NATRL complex is −8.2 ± 0.4 kcal/mol and slightly less compared to −8.4 kcal/mol for PDZ1−NATRL. Thus, there is no significant difference between complexes of wild type PDZ1−NDSLL and the Glu43Asp mutant. This finding may be due to the absence of contact between Arg^{-1} and Glu43Asp and can be compensated by interactions of Asn^{-4} with PDZ1Glu43Asp. In our model, the side chain of Asn^{-4} makes a sharp angle and may interact with PDZ1Glu43Asp.

The computed binding energy of PDZ2 to −WETVM equals −9.5 ± 0.4 kcal/mol. A decrease in the binding energy in going from PDZ2−WETVM to PDZ1−WETVM could be accounted for by exchange of His at position 27 in PDZ1 to Asn at position 167 in PDZ2 (see Figures 1B and 3A). Our results agree with experimentally measured K_d values for the binding of PDZ1 to the tetrapeptide −DTRL (948 nM) or hexapeptide −VQDTRL (365 nM) of the CFTR carboxy-terminus,[13] which corresponds to binding energies of −8.2 and −8.8 kcal/mol, respectively (Table 4). The measured binding energy of PDZ2 to the hexapeptide −VQDTRL equals −8.1 kcal/mol (1079 nM[13]). As shown theoretically[57] and experimentally,[13,37] PDZ1 binds with higher affinity to the target ligands than does PDZ2, and our calculations reveal a similar trend.

The present results show that Trp^{-4} and Leu^{-4} contact His72 in the α2 helix of PDZ1 and His212 in the α2 helix of PDZ2 rather than interacting with the residues from the top of the β2 strand or the β2−β3 loop. The β2− β3 loop is not involved in the hydrogen bond network and exhibits a high degree of mobility, especially for PDZ1−NATRL (see residues 31−34 in Figure S7 of the Supporting Information). This observation is in agreement with both the calculated binding energy between PDZ1 and the −NATRL peptide (Table 4) and the hydrogen bond analysis, which confirms the absence of interactions of the −NATRL at positions −3 and −4. It is clear that the lack of interactions at Ala^{-3} and Asn^{-4} destabilize the PDZ−NATRL complex.

A hydrogen bond analysis reveals that Gly30 from the top of the β2 strand of PDZ1 forms a hydrogen bond with the backbone oxygen atom of Asn^{-4} of PDZ1−NDSLL and, therefore, can further stabilize the complex at position −4. In the case of PDZ2, Ser170 is not involved directly in the interactions with Trp^{-4} of −WETVM or Leu^{-4} of −LFSNL ligands but rather with Gln177 (both Ser170 and Gln177 have a low RMSF value; see Figure S7B of the Supporting Information). Gln177 forms a hydrogen bond with His212, which is involved in the interactions with Ser^{-2} or Thr^{-2} and Trp^{-4} or Leu^{-4}. We propose that this explains why Ser170 is not a phosphorylation site in PDZ2. Ser173 from the top of the β2−β3 loop, in contrast, is exposed to the surface and is extremely mobile (Figure S7B of the Supporting Information), conditions favorable for phosphorylation.

The modeling of the self-associated conformation, where PDZ2 interacts with EB, reveals that PDZ2 recognizes the −LFSNL motif with a binding affinity of −8.8 ± 0.4 kcal/mol (Table 4). This agrees with the experimental data for self-association of NHERF1.[59] The reported K_d of 1−10 μM[59] corresponds to the binding energy in the range of −8.3 to −6.8 kcal/mol. Several experimental studies reported that the carboxy-terminus of NHERF1 is highly flexible and disordered in solution. Cheng et al.[12] described *in vitro* NMR results with isolated PDZ2-CT that provides evidence that the EB ligand of NHERF1 adopts a helical conformation when engaged with PDZ2. It is not completely clear whether the disordered carboxy-terminus remains unstructured *in vivo* or may become more structured in the cell. In our study, the carboxy-terminus of NHERF1 (−LFSNL) assumes an extended conformation. We propose that a disordered ensemble may consist of a set of energetically favorable conformations. Therefore, the carboxy-terminal region of NHERF1 may exist in dynamic equilibrium between disordered and helical structures.

Overall, our results demonstrate important roles for electrostatic interactions in the binding between the NHERF1 PDZ domains with a range of ligands, consistent with previous reports.[60] In contrast, Basdevant et al.[61] showed that the electrostatic component has a negligible effect on the binding of the −EDSFL, −NDSLL, and −QDTRL ligands to NHERF1 PDZ1. However, the investigated peptides contain charged amino acid residues that are positioned to make favorable interactions with the positively charged side chain of Arg40 of PDZ1 as we verified here using the PDZ1−NDSLL and PDZ1−WETVM complexes. The NHERF1 PDZ2 domain also exhibits a preference for ligands containing a negatively charged side chain at position −3. Our results also reveal that PDZ1 has a higher affinity for −WETVM than does PDZ2. The same trend was observed experimentally for the SVIM motif of AQP9.[25] We speculate that Ile^{-1} of SVIM may be involved in the hydrophobic interactions with His27 of PDZ1 and, therefore, contribute to the binding affinity of PDZ1. Thus, His27 of PDZ1 may play a more significant role in the ligand binding than previously appreciated.[58]

We assume that the zero salt conditions employed here slightly overestimate the binding affinity of PDZ1 or PDZ2 with the tested ligands. Binding affinities of ligands for the syntrophin PDZ domain, another member of the PDZ family, decrease in a linear fashion with increasing ionic strength.[60] However, mutation of a highly conserved, positively charged residue in the binding pocket, which makes contact with the peptide carboxylate group, does not affect the salt dependence of binding. On the basis of these findings, we did not observe an appreciable dependence of binding affinity on the salt concentration.

In conclusion, the distinct binding affinity of PDZ1 and PDZ2 to cognate peptides containing a PDZ-recognition motif has been characterized by MD simulation. The interactions between the PDZ1 and PDZ2 domains and the peptides studied reveal common features. Both PDZ1 and PDZ2 form multiple hydrophobic and hydrogen bond interactions with the carboxy-terminal PDZ-recognition motifs. For the peptides studied, the charge interactions with PDZ1 have a profound impact on ligand binding. Specificity in the PDZ1−ligand interaction may derive from residues outside the binding pocket. Arg40, His27, and Glu43 are essential for the formation of salt bridges with peptides having corresponding negatively or positively charged residues at position −3 and −1, respectively. The electrostatic nature of the salt bridges was confirmed by MD simulation of His27Ala and Glu43Asp variants of PDZ1. With the exception of Arg180, no such essential residues are present in PDZ2, and the modeling suggests that these key residues may contribute to the higher binding affinity of PDZ1 compared to that of PDZ2. Thus, electrostatic steering can regulate the proper balance of the PDZ1 and PDZ2 binding specificity and, therefore, their unique function.

■ ASSOCIATED CONTENT

Supporting Information

Summary of modeling systems, equilibration, and production simulation time, and rmsd); PDZ1-NDSLL/Val, PDZ1-NDSLL/Ala, and PDZ1−NATRL; PDZ2-WETVM; PDZ2-LFSNL; amino acid sequence of NHERF1 PDZ1 (PDB code: 1GO4) and PDZ2 (PDB code: 2OZF); evolution of the rmsd of the C_α atoms with respect to the initial conformation during equilibration simulation for the PDZ1-WETVM, PDZ1−NATRL, PDZ2-WETVM, and PDZ2-LFSNL complexes; rms fluctuations for the PDZ1- and PDZ2-ligand systems; variation of the binding energies with production simulation time for PDZ1-WETVM, PDZ1−NATRL, PDZ2-WETVM, and PDZ2-LFSNL; evolution of the rmsd of the C_α atoms with respect to the initial conformation during equilibration simulation for the mutated PDZ1-NDSLL/A and PDZ1-NDSLL/V complexes; time evolution of the distance between the carboxylic group of Glu^{-3}/Asp^{-3} and His27 or Arg40 for the PDZ1-WETVM and PDZ1-NDSLL complexes, respectively; and interaction network between the carboxylate oxygens of Glu^{-3} of the −WETVM peptide and the hydrogen atoms of Arg40, His27, and His29 (only side chains are presented) of PDZ1. This material is available free of charge via the Internet at http://pubs.acs.org.

■ AUTHOR INFORMATION

Corresponding Author

*University of Pittsburgh School of Medicine, Department of Pharmacology & Chemical Biology, W1340 Biomedical Science Tower, 200 Lothrop Street, Pittsburgh, PA 15261, USA. Tel: 1.412.383.7783. E-mail: paf10@pitt.edu.

Funding

This research was supported by grants DK069998 and DK069998-04S1 from the National Institutes of Health.

Notes

The authors declare no competing financial interest.

■ ACKNOWLEDGMENTS

The calculations were performed with resources at the Pittsburgh Supercomputing Center.

■ ABBREVIATIONS

NHERF1, Na^+/H^+ exchange regulatory factor-1; EBD, ezrin-binding domain; Npt2a, type II sodium-dependent phosphate cotransporters; β2-AR, β2-adrenergic receptor; PTHR, parathyroid hormone receptor; EB, carboxy-terminal PDZ ligand; MD, molecular dynamics; PDZ, postsynaptic density 95/disk large/zona occludens; CT, carboxy-terminus; CFTR, cystic fibrosis transmembrane regulator; GRK6, G-protein-coupled receptor kinase 6; PDGFR, platelet-derived growth factor receptor; *NPT*, constant pressure, temperature, and number of particles; *NVT*, constant volume, temperature, and number of particles; PME, particle mesh Ewald; rmsd, root-mean-square fluctuation; RMSF, root-mean-square fluctuation; SIE, solvated interaction energy; H-bond, hydrogen bond; PDB, Protein Data Bank

■ REFERENCES

(1) Seidler, U., Singh, A. K., Cinar, A., Chen, M. M., Hillesheim, J., Hogema, B., and Riederer, B. (2009) The role of the NHERF Family of PDZ scaffolding proteins in the regulation of salt and water transport. *Ann. N.Y. Acad. Sci. 1165*, 249−260.

(2) Sheng, M., and Sala, C. (2001) PDZ domains and the organization of supramolecular complexes. *Annu. Rev. Neurosci. 24*, 1−29.

(3) Thelin, W. R., Hodson, C. A., and Milgram, S. L. (2005) Beyond the brush border: NHERF4 blazes new NHERF turf. *J. Physiol. 567*, 13−19.

(4) Hung, A. Y., and Sheng, M. (2002) PDZ domains: structural modules for protein complex assembly. *J. Biol. Chem. 277*, 5699−5702.

(5) Stiffler, M. A., Chen, J. R., Grantcharova, V. P., Lei, Y., Fuchs, D., Allen, J. E., Zaslavskaia, L. A., and MacBeath, G. (2007) PDZ domain binding selectivity is optimized across the mouse proteome. *Science 317*, 364−369.

(6) Songyang, Z., Fanning, A. S., Fu, C., Xu, J., Marfatia, S. M., Chishti, A. H., Crompton, A., Chan, A. C., Anderson, J. M., and Cantley, L. C. (1997) Recognition of unique carboxyl-terminal motifs by distinct PDZ domains. *Science 275*, 73−77.

(7) Fouassier, L., Yun, C. C., Fitz, J. G., and Doctor, R. B. (2000) Evidence for ezrin-radixin-moesin-binding phosphoprotein 50 (EBP50) self-association through PDZ-PDZ interactions. *J. Biol. Chem. 275*, 25039−25045.

(8) Lau, A. G., and Hall, R. A. (2001) Oligomerization of NHERF-1 and NHERF-2 PDZ domains: differential regulation by association with receptor carboxyl-termini and by phosphorylation. *Biochemistry 40*, 8572−8580.

(9) Morales, F. C., Takahashi, Y., Momin, S., Adams, H., Chen, X., and Georgescu, M. M. (2007) NHERF1/EBP50 head-to-tail intramolecular interaction masks association with PDZ domain ligands. *Mol. Cell. Biol. 27*, 2527−2537.

(10) Bhattacharya, S., Dai, Z. P., Li, J. Q., Baxter, S., Callaway, D. J. E., Cowburn, D., and Bu, Z. M. (2010) A Conformational switch in the scaffolding protein NHERF1 controls autoinhibition and complex formation. *J. Biol. Chem. 285*, 9981−9994.

(11) Karthikeyan, S., Leung, T., and Ladias, J. A. (2002) Structural determinants of the Na^+/H^+ exchanger regulatory factor interaction with the ß$_2$ adrenergic and platelet-derived growth factor receptors. *J. Biol. Chem. 277*, 18973−18978.

(12) Cheng, H., Li, J. Q., Fazlieva, R., Dai, Z. P., Bu, Z. M., and Roder, H. (2009) Autoinhibitory Interactions between the PDZ2 and C-terminal domains in the scaffolding protein NHERF1. *Structure 17*, 660−669.

(13) Cushing, P. R., Fellows, A., Villone, D., Boisguerin, P., and Madden, D. R. (2008) The relative binding affinities of PDZ partners for CFTR: a biochemical basis for efficient endocytic recycling. *Biochemistry 47*, 10084−10098.

(14) Li, J. Q., Poulikakos, P. I., Dai, Z. P., Testa, J. R., Callaway, D. J. E., and Bu, Z. M. (2007) Protein kinase c phosphorylation disrupts Na^+/H^+ exchanger regulatory factor 1 autoinhibition and promotes cystic fibrosis transmembrane conductance regulator macromolecular assembly. *J. Biol. Chem. 282*, 27086−27099.

(15) Mahon, M. J., and Segre, G. V. (2004) Stimulation by parathyroid hormone of a NHERF-1-assembled complex consisting of the parathyroid hormone I receptor, phospholipase C beta, and actin increases intracellular calcium in opossum kidney cells. *J. Biol. Chem. 279*, 23550−23558.

(16) Short, D. B., Trotter, K. W., Reczek, D., Kreda, S. M., Bretscher, A., Boucher, R. C., Stutts, M. J., and Milgram, S. L. (1998) An apical PDZ protein anchors the cystic fibrosis transmembrane conductance regulator to the cytoskeleton. *J. Biol. Chem. 273*, 19797−19801.

(17) Hall, R. A., Spurney, R. F., Premont, R. T., Rahman, N., Blitzer, T., Pitcher, J. A., and Lefkowitz, R. J. (1999) G protein-coupled receptor kinase 6A phosphorylates the Na^+/H^+ exchanger regulatory factor via a PDZ domain-mediated interaction. *J. Biol. Chem. 274*, 24328−24334.

(18) Lee, J. H., Richter, W., Namkung, W., Kim, K. H., Kim, E., Conti, M., and Lee, M. G. (2007) Dynamic regulation of cystic fibrosis transmembrane conductance regulator by competitive interactions of molecular adaptors. *J. Biol. Chem. 282*, 10414−10422.

(19) Ardura, J. A., and Friedman, P. A. (2011) Regulation of G protein-coupled receptor function by Na^+/H^+ exchange regulatory factors. *Pharmacol. Rev. 63*, 882−900.

(20) Khundmiri, S. J., Ahmad, A., Bennett, R. E., Weinman, E. J., Steplock, D., Cole, J., Baumann, P. D., Lewis, J., Singh, S., Clark, B. J., and Lederer, E. D. (2008) Novel regulatory function for NHERF-1 in Npt2a transcription. *Am. J. Phys. Renal Physiol. 294*, F840−F849.

(21) Hernando, N., Deliot, N., Gisler, S. M., Lederer, E., Weinman, E. J., Biber, J., and Murer, H. (2002) PDZ-domain interactions and apical expression of type IIa Na/P-i cotransporters. *Proc. Natl. Acad. Sci. U.S.A. 99*, 11957−11962.

(22) Hall, R. A., Ostedgaard, L. S., Premont, R. T., Blitzer, J. T., Rahman, N., Welsh, M. J., and Lefkowitz, R. J. (1998) A C-terminal motif found in the ß$_2$-adrenergic receptor, P2Y1 receptor and cystic fibrosis transmembrane conductance regulator determines binding to the Na^+/H^+ exchanger regulatory factor family of PDZ proteins. *Proc. Natl. Acad. Sci. U.S.A. 95*, 8496−8501.

(23) Breton, S., Wiederhold, T., Marshansky, V., Nsumu, N. N., Ramesh, V., and Brown, D. (2000) The B1 subunit of the H^+ATPase is a PDZ domain-binding protein: Colocalization with NHE-RF in renal B-intercalated cells. *J. Biol. Chem. 275*, 18219−18224.

(24) Voltz, J. W., Weinman, E. J., and Shenolikar, S. (2001) Expanding the role of NHERF, a PDZ-domain containing protein adapter, to growth regulation. *Oncogene 20*, 6309−6314.

(25) Pietrement, C., Da Silva, N., Silberstein, C., James, M., Marsolais, M., Van Hoek, A., Brown, D., Pastor-Soler, N., Ameen, N., Laprade, R., Ramesh, V., and Breton, S. (2008) Role of NHERF1, cystic fibrosis transmembrane conductance regulator, and cAMP in the regulation of aquaporin 9. *J. Biol. Chem. 283*, 2986−2996.

(26) Sneddon, W. B., Syme, C. A., Bisello, A., Magyar, C. E., Weinman, E. J., Rochdi, M. D., Parent, J. L., Abou-Samra, A. B., and Friedman, P. A. (2003) Activation-independent parathyroid hormone receptor internalization is regulated by NHERF1 (EBP50). *J. Biol. Chem. 278*, 43787−43796.

(27) Wang, B., Yang, Y., and Friedman, P. A. (2008) Na/H Exchange regulator factor 1, a novel Akt-associating protein, regulates extracellular signal-related signaling through a B-Raf-mediated pathway. *Mol. Biol. Cell 19*, 1637−1645.

(28) Wang, B., Bisello, A., Yang, Y., Romero, G. G., and Friedman, P. A. (2007) NHERF1 regulates parathyroid hormone receptor membrane retention without affecting recycling. *J. Biol. Chem. 282*, 36214−36222.

(29) Wheeler, D. G., Sneddon, W. B., Wang, B., Friedman, P. A., and Romero, G. (2007) NHERF-1 and the cytoskeleton regulate the traffic and membrane dynamics of G protein-coupled receptors. *J. Biol. Chem. 282*, 25076−25087.
(30) Wheeler, D., Garrido, J. L., Bisello, A., Kim, Y. K., Friedman, P. A., and Romero, G. (2008) Regulation of PTH1R dynamics, traffic and signaling by the Na^+/H^+ exchanger regulatory factor-1 (NHERF1) in rat osteosarcoma ROS 17/28 cells. *Mol. Endocrinol. 22*, 1163−1170.
(31) Wang, B., Yang, Y., Abou-Samra, A. B., and Friedman, P. A. (2009) NHERF1 regulates parathyroid hormone receptor desensitization; interference with ß-arrestin binding. *Mol. Pharmacol. 75*, 1189−1197.
(32) Klenk, C., Vetter, T., Zurn, A., Vilardaga, J. P., Friedman, P. A., Wang, B., and Lohse, M. J. (2010) NHERF1, ß-arrestin, and the parathyroid hormone receptor form a ternary signaling complex. *J. Biol. Chem. 285*, 30355−30362.
(33) Wang, B., Ardura, J. A., Romero, G., Yang, Y., Hall, R. A., and Friedman, P. A. (2010) Na/H exchanger regulatory factors control PTH receptor signaling by differential activation of Gα protein subunits. *J. Biol. Chem. 285*, 26976−26986.
(34) Mahon, M. J., Donowitz, M., Yun, C. C., and Segre, G. V. (2002) Na^+/H^+ exchanger regulatory factor 2 directs parathyroid hormone 1 receptor signalling. *Nature 417*, 858−861.
(35) Wheeler, D., Garrido, J. L., Bisello, A., Kim, Y. K., Friedman, P. A., and Romero, G. (2008) Regulation of parathyroid hormone type 1 receptor dynamics, traffic, and signaling by the Na^+/H^+ exchanger regulatory factor-1 in rat osteosarcoma ROS 17/2.8 cells. *Mol. Endocrinol. 22*, 1163−1170.
(36) Terawaki, S., Maesaki, R., and Hakoshima, T. (2006) Structural basis for NHERF recognition by ERM proteins. *Structure 14*, 777−789.
(37) Gisler, S. M., Kittanakom, S., Fuster, D., Wong, V., Bertic, M., Radanovic, T., Hall, R. A., Murer, H., Biber, J., Markovich, D., Moe, O. W., and Stagljar, I. (2008) Monitoring protein-protein interactions between the mammalian integral membrane transporters and PDZ-interacting partners using a modified split-ubiquitin membrane yeast two-hybrid system. *Mol. Cell. Proteomics 7*, 1362−1377.
(38) Kurnikov, I. Hamiltonian to research large molecules (HARLEM), http://www.harlemprog.org.
(39) Case, D. A., Darden T. A., Cheatham, T. E., III, Simmerling, C. L., Wang, J., Duke, R. E., Luo, R. C. W., Merz, K. M., Pearlman, D. A., Crowley, M., Walker, R. C., Zhang, W., Wang, B., Hayik, S., Roitberg, A., Seabra, G., Wong, K. F., Paesani, F., Wu, X., Brozell, S. R., Tsui, V., Gohlke, H., Tan, C., Mongan, J., Hornak, V., Cui, G., Beroza, P., Mathews, D. H., Schafmeister, W. S. R., Kollman, P. A. (2006) *AMBER 9*, University of California, San Francisco, CA.
(40) Jorgensen, W. L., Chandrasekhar, J., Madura, J. D., Impey, R. W., and Klein, M. L. (1983) Comparison of simple potential functions for simulating liquid water. *J. Chem. Phys. 79*, 926−935.
(41) Case D. A., Darden, T., Cheatham T. E., III, Simmerling C. L., Wang, J., Duke, R. E., Luo, R., Crowley, M., Walker, R. C., Zhang, W., Merz, K. M., Wang, B., Hayik, S., Roitberg, A., Seabra, G., Kolossváry, I., Wong, K. F., Paesani, F., Vanicek, J., Wu, X., Brozell, S. R., Steinbrecher, T., Gohlke, H, Yang, L., Tan, C., Mongan, J., Hornak, V., Cui, G., Mathews, D. H., Seetin, M. G., Sagui, C., Babin, V., Kollman, P. A. (2008) *AMBER 10*, University of California, San Francisco, CA.
(42) Cornell, W. D., Cieplak, P., Bayly, C. I., Gould, I. R., Merz, K. M., Ferguson, D. M., Spellmeyer, D. C., Fox, T., Caldwell, J. W., and Kollman, P. A. (1995) A second generation force field for the simulation of proteins, nucleic acids, and organic molecules. *J. Am. Chem. Soc. 117*, 5179−5197.
(43) Berendsen, H. J. C., Postma, J. P. M, Vangunsteren, W. F., Dinola, A., and Haak, J. R. (1984) Molecular dynamics with coupling to an external bath. *J. Chem. Phys. 81*, 3684−3690.
(44) Darden, T., York, D., and Pedersen, L. (1993) Particle mesh Ewald: an N·log(N) method for Ewald sums in large systems. *J. Chem. Phys. 98*, 10089−10092.
(45) Ryckaert, J. P. (1977) Numerical integration of Cartesian equations of motion of a system with constraints: molecular dynamics of n-alkanes. *J. Comput. Phys. 23*, 327.
(46) Naim, M., Bhat, S., Rankin, K. N., Dennis, S., Chowdhury, S. F., Siddiqi, I., Drabik, P., Sulea, T., Bayly, C. I., Jakalian, A., and Purisima, E. O. (2007) Solvated interaction energy (SIE) for scoring protein-ligand binding affinities. 1. Exploring the parameter space. *J. Chem. Inf. Model. 47*, 122−133.
(47) Kollman, P. A., and Massova, I. (2000) Combined molecular mechanical and continuum solvent approach (MM-PBSA/GBSA) to predict ligand binding. *Perspect. Drug Discovery Des. 18*, 113−135.
(48) Mamonova, T., Yonkunas, M. J., and Kurnikova, M. G. (2008) Energetics of the cleft closing transition and the role of electrostatic interactions in conformational rearrangements of the glutamate receptor ligand binding domain. *Biochemistry 47*, 11077−11085.
(49) Cui, Q. Z., Sulea, T., Schrag, J. D., Munger, C., Hung, M. N., Naim, M., Cygler, M., and Purisima, E. O. (2008) Molecular dynamics-solvated interaction energy studies of protein-protein interactions: the MP1-p14 scaffolding complex. *J. Mol. Biol. 379*, 787−802.
(50) Yang, B., Hamza, A., Chen, G. J., Wang, Y., and Zhan, C. G. (2010) Computational determination of binding structures and free energies of phosphodiesterase-2 with benzo [1,4] diazepin-2-one derivatives. *J. Phys. Chem. B 114*, 16020−16028.
(51) Mamonova, T., Hespenheide, B., Straub, R., Thorpe, M. F., and Kurnikova, M. (2005) Protein flexibility using constraints from molecular dynamics simulations. *Phys. Biol. 2*, S137−S147.
(52) Mcdonald, I. K., and Thornton, J. M. (1994) Satisfying hydrogen bonding potential in proteins. *J. Mol. Biol. 238*, 777−793.
(53) Stickle, D. F., Presta, L. G., Dill, K. A., and Rose, G. D. (1992) Hydrogen bonding in globular proteins. *J. Mol. Biol. 226*, 1143−1159.
(54) Jacobs, D. J., Rader, A. J., Kuhn, L. A., and Thorpe, M. F. (2001) Protein flexibility predictions using graph theory. *Protein Struct., Funct. Bioinf. 44*, 150−165.
(55) Karthikeyan, S., Leung, T., Birrane, G., Webster, G., and Ladias, J. A. A. (2001) Crystal structure of the PDZ1 domain of human Na^+/H^+ exchanger regulatory factor provides insights into the mechanism of carboxyl-terminal leucine recognition by class I PDZ domains. *J. Mol. Biol. 308*, 963−973.
(56) Appleton, B. A., Zhang, Y. N., Wu, P., Yin, J. P., Hunziker, W., Skelton, N. J., Sidhu, S. S., and Wiesmann, C. (2006) Comparative structural analysis of the Erbin PDZ domain and the first PDZ domain of ZO-1. Insights into determinants of PDZ domain specificity. *J. Biol. Chem. 281*, 22312−22320.
(57) Tandon, C., De Lisle, R. C., Boulatnikov, I., and Naik, P. K. (2007) Interaction of carboxyl-terminal peptides of cytosolic-tail of apactin with PDZ domains of NHERF/EBP50 and PDZK-1/CAP70. *Mol. Cell. Biochem. 302*, 157−167.
(58) Mayasundari, A., Ferreira, A. M., He, L., Mahindroo, N., Bashford, D., and Fujii, N. (2008) Rational design of the first small-molecule antagonists of NHERF1/EBP50 PDZ domains. *Bioorg. Med. Chem. Lett. 18*, 942−945.
(59) Shenolikar, S., Minkoff, C. M., Steplock, D. A., Evangelista, C., Liu, M. Z., and Weinman, E. J. (2001) N-terminal PDZ domain is required for NHERF dimerization. *FEBS Lett. 489*, 233−236.
(60) Harris, B. Z., Lau, F. W., Fujii, N., Guy, R. K., and Lim, W. A. (2003) Role of electrostatic interactions in PDZ domain ligand recognition. *Biochemistry 42*, 2797−2805.
(61) Ceruso, M., Basdevant, N., and Weinstein, H. (2006) Thermodynamic basis for promiscuity and selectivity in protein-protein interactions: PDZ domains, a case study. *J. Am. Chem. Soc. 128*, 12766−12777.